

## Pseudo-Bimolecular [2+2] Cycloaddition Studied by Time-Resolved Photoelectron Spectroscopy

Rasmus Y. Brogaard,<sup>[a, d]</sup> Andrey E. Boguslavskiy,<sup>[a]</sup> Oliver Schalk,<sup>[a]</sup> Gary D. Enright,<sup>[a]</sup> Henning Hopf,<sup>[b]</sup> Vitaly A. Raev,<sup>[b]</sup> Peter G. Jones,<sup>[c]</sup> Ditte L. Thomsen,<sup>[d]</sup> Theis I. Sølling,<sup>\*, [d]</sup> and Albert Stolow<sup>\*, [a]</sup>

**Abstract:** The first study of pseudo-bimolecular cycloaddition reaction dynamics in the gas phase is presented. We used femtosecond time-resolved photoelectron spectroscopy (TRPES) to study the [2+2] photocycloaddition in the model system pseudo-*gem*-divinyl[2.2]paracyclophane. From X-ray crystal diffraction measurements we found that the ground-state molecule can exist in two conformers; a reactive one in which the vinyl groups are immediately situated for [2+2] cycloaddition and a nonreactive confor-

mer in which they point in opposite directions. From the measured S<sub>1</sub> lifetimes we assigned a clear relation between the conformation and the excited-state reactivity; the reactive conformer has a lifetime of 13 ps, populating the ground state through a conical intersection leading to [2+2] cyclo-

addition, whereas the nonreactive conformer has a lifetime of 400 ps. Ab initio calculations were performed to locate the relevant conical intersection (CI) and calculate an excited-state [2+2] cycloaddition reaction path. The interpretation of the results is supported by experimental results on the similar but nonreactive pseudo-*para*-divinyl[2.2]paracyclophane, which has a lifetime of more than 500 ps in the S<sub>1</sub> state.

**Keywords:** ab initio calculations · cycloaddition · cyclophanes · photochemistry · photoelectron spectroscopy

### Introduction

The molecular mechanisms underlying the photophysical properties of DNA are a subject of growing interest.<sup>[1,2]</sup> The chemical stability of DNA when exposed to UV light is remarkably high as compared to other organic molecules, leading to the suggestion that this factor has been crucial in the natural evolution of the DNA bases.<sup>[1,3–6]</sup> The main reason for the photostability of DNA is the existence of ultrafast, nonradiative relaxation pathways that convert “dangerous” excited-state electronic energy to “safe” vibrational energy in the ground state.<sup>[1,2,4,6–10]</sup> In electronically excited

states chemical reactions are more likely to occur due to their particular charge distributions. In the vibrationally excited ground state, on the other hand, excess energy can readily be dissipated as heat into the solvent. This mechanism of effectively transferring the photon energy into heat fails when excited-state reactions occur on the same time-scale as the nonradiative protection mechanisms. The most common excited-state reaction in DNA is the formation of the cyclobutane pyrimidine dimer in a [2+2] cycloaddition between adjacent thymine bases,<sup>[11,12]</sup> a mutation that can lead to skin cancer.<sup>[13,14]</sup> This reaction has been studied by Schreier et al.<sup>[15]</sup> in an all-thymine oligodeoxynucleotide by using femtosecond (fs) time-resolved infrared spectroscopy, revealing that the reaction is complete within 1 ps. Such a high reaction rate would be lethal for DNA if all adjacent thymine bases underwent [2+2] cycloaddition. This is obviously not the case and the remarkably low quantum yield for this reaction is explained by a conformational restriction: a reactive conformation of the thymine bases before light absorption is crucial for inducing the ultrafast mutagenic cycloaddition.<sup>[15]</sup> This interplay between conformational dynamics and excited-state reactivity in photochemistry has been long appreciated.<sup>[16]</sup> Recently, we have studied this phenomenon in a series of organic molecules by using both computational and fs time-resolved experimental methods.<sup>[17–21]</sup> In the Hofmann–Löffler and Barton reactions, where the key 1,5-hydrogen transfer step of the reaction has to be preceded by a conformational change, no ultrafast reactivity is observed.<sup>[19–21]</sup> In 1,3-dibromopropane, the photo-

[a] R. Y. Brogaard, Dr. A. E. Boguslavskiy, Dr. O. Schalk, Dr. G. D. Enright, Prof. A. Stolow  
Stacie Institute for Molecular Sciences  
National Research Council (Canada), 100 Sussex Drive  
Rm 2067, Ottawa, ON, K1A 0R6 (Canada)  
Fax: (+1) 613-991-3437  
E-mail: Albert.Stolow@nrc-cnrc.gc.ca

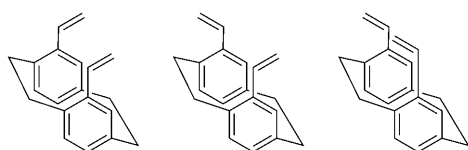
[b] Prof. H. Hopf, Dr. V. A. Raev  
Institute of Organic Chemistry  
Braunschweig University of Technology (Germany)

[c] Prof. P. G. Jones  
Institute of Inorganic and Analytical Chemistry  
Braunschweig University of Technology (Germany)

[d] R. Y. Brogaard, D. L. Thomsen, Dr. T. I. Sølling  
Department of Chemistry, University of Copenhagen  
Universitetsparken 5, B506, 2100 København Ø (Denmark)  
Fax: (+45) 353-20212  
E-mail: theis@kiku.dk

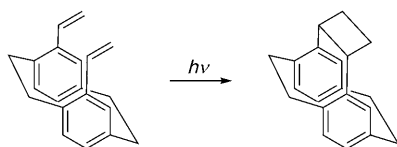
dissociation of a highly excited Rydberg state takes place through a coupling to a dissociative valence state, a coupling that is significantly modulated by the conformation of the  $\text{CH}_2\text{Br}$  groups.<sup>[17,18]</sup>

In this work, we aim for a better understanding of photo-induced [2+2] cycloaddition dynamics, especially with respect to the relation between the ground-state conformation prior to light absorption and the resulting excited-state reactivity. Recently, pseudo-geminally disubstituted [2.2]paracyclophanes were shown to be well suited for studying the interaction between functional groups.<sup>[22]</sup> Thus, we have chosen pseudo-*gem*-divinyl[2.2]paracyclophane (GEM), shown in Scheme 1, as a model system for the [2+2] photo-



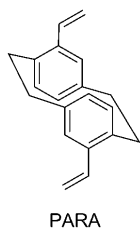
Scheme 1. The three conformers of pseudo-*gem*-divinyl[2.2]paracyclophane. From left to right: *anti-anti*, *syn-anti*, and *syn-syn*.

cycloaddition. As shown in Scheme 1, the molecule can in principle exist in three different conformers depending on the relative orientation of the vinyl groups: the *anti-anti*, *syn-syn*, and *syn-anti* conformers. In benzene the molecule cyclizes quantitatively upon irradiation with a UV lamp. It does so even when left in diffuse daylight.<sup>[22]</sup> As indicated in Scheme 2, the cyclized product is formed only from the



Scheme 2. The photoinduced [2+2] cycloaddition in GEM.

*anti-anti* conformer. Thus, GEM seems to be a good candidate for comparing the excited-state dynamics of two different types of conformers: one that is suited for [2+2] cycloaddition and one that is not. Except for 1,3-dibromopropane, the molecules studied previously must undergo significant conformational changes to reach the reactive conformation. With the use of the [2.2]paracyclophane scaffold, this is no longer the case; the ethylene units are well situated for photoinduced [2+2] cycloaddition. We have also studied the isomeric pseudo-*para*-divinyl[2.2]paracyclophane (PARA). In PARA the vinyl groups are oriented such that



the [2+2] cycloaddition cannot take place. PARA thus serves as a non-reactive reference compound for comparison with GEM. Here, we study the excited-state dynamics of the isolated molecules by using time-resolved photoelectron spectroscopy<sup>[23–34]</sup> (TRPES), supplemented by *ab initio* calculations.

## Results

**Crystal structure determination:** The obtained structures are shown in Figure 1. In the crystal structure of GEM, the *anti-anti* and the *syn-anti* conformers are present in the

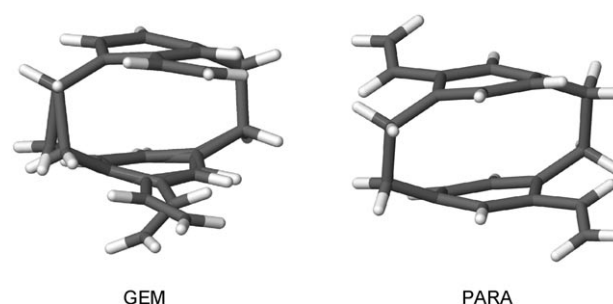


Figure 1. Crystal structures of GEM (two conformers overlaid) and PARA as obtained from X-ray diffraction measurements.

ratio 73:27 (shown as overlaid structures). In the crystal structure of PARA, two independent molecules are present. The molecules both possess inversion symmetry and are closely similar (root-mean-square (r.m.s.) deviation of all non-hydrogen atoms is 0.02 Å). For simplicity, only one of these structures is shown in Figure 1.

**Gas-phase UV/Vis absorption spectra:** The absorption spectra of GEM and PARA are shown in Figure 2. In the spectrum of GEM the region around 280–340 nm reveals two

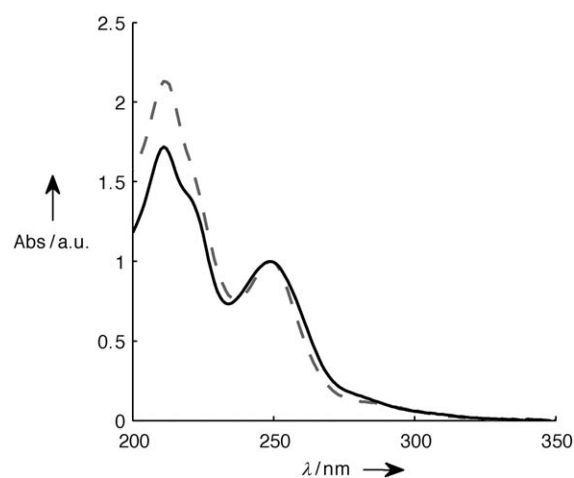


Figure 2. Absorption spectra of GEM (----) and PARA (—) arbitrarily normalized to the peak at 249 nm.

weak, barely distinguishable features with maxima around 285 and 315 nm (not visible in Figure 2). Further to the blue part of the spectrum there is a stronger and better defined maximum at 249 nm.

The position of the absorption maxima in the spectrum of PARA are very close to those of GEM, indicating that the difference in the electronic structure at the Franck–Condon (FC) geometry between PARA and GEM is minor. This supports the use of PARA as the non-reactive counterpart to GEM.

### Ab initio calculations

*Pseudo-gem-divinyl[2.2]paracyclophane*: The optimized geometry of the *anti-anti* conformer of GEM is shown in Figure 3 (left). Note that the molecule does not possess  $C_s$

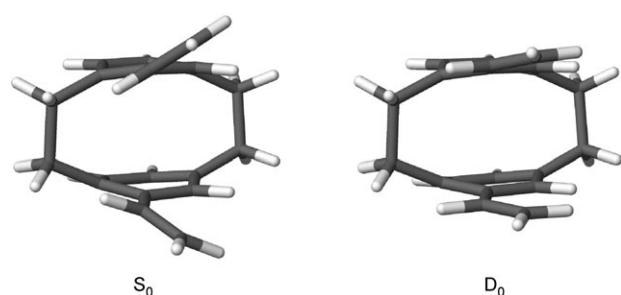


Figure 3. B3LYP/6-31G(d)-optimized geometries of the *anti-anti* conformer of GEM in the neutral ground state ( $S_0$ ) and the cation ground state ( $D_0$ ).

symmetry; the two halves are twisted, reducing the symmetry to  $C_1$ . This distortion was also observed in previous computational and experimental studies of [2.2]paracyclophane.<sup>[35–37]</sup> An important point to notice is that the vinyl groups are twisted by  $26^\circ$  out of the plane of the phenyl rings. The twist angles in the *syn-anti* conformer (not shown) are similar. Comparison of the calculated structures and the crystal structures presented above is not straightforward, because the former represent gas phase structures, whereas the latter are solid-state structures. The twist of the two halves that reduces the symmetry is also observed in the crystal structure. On the other hand, there is a considerable difference between the calculated and the crystal structures with respect to the twist angles of the vinyl groups. This difference could be due to limited space in the crystal lattice, that constraints the vinyl-group twist angles. This constraint is not present in the gas phase, which, in our opinion, means that detailed comparison between the calculated and the crystal structures should not be overestimated.

It would be desirable to be able to calculate the heats of formation of the calculated *anti-anti* and *syn-anti* geometries and to predict on this basis a ratio of the *anti-anti* to *syn-anti* conformers. But this would require calculation of heats of formation within chemical accuracy, which to the best of our knowledge is not possible for molecules as large

as the paracyclophanes. Furthermore, this ratio ( $\approx 3:1$ ) is available from the X-ray data presented above. If the conformers would equilibrate after sublimation of the sample from the crystalline phase, the ratio could change in the gas phase. Based on the calculation of the vinyl twist transition state involved in the conversion between the *anti-anti* and *syn-anti* conformer, we find that the electronic-energy barrier on the B3LYP/6-31G(d) level is  $10 \text{ kJ mol}^{-1}$ , which is considerably more than  $k_B T$  at  $120^\circ\text{C}$ . Thus, we believe that the conformer ratio present in the crystal will be preserved in the gas phase after sublimation.

In the ionic ground state (Figure 3, right), the vinyl groups are almost in plane with the ring, the twist angle being reduced to  $7^\circ$ . The difference in the twist angles between the ground and ionic states is expected to result in an extended Franck–Condon progression in the photoelectron (PE) spectrum as was previously observed for substituted styrenes.<sup>[38]</sup>

To explore the electronic character of the excited states in the FC region, vertical excitations of the *anti-anti* and *syn-anti* conformers were calculated. The calculated excitation energies are shown in Table 1, together with approximate

Table 1. RI-CC2/cc-pVDZ excitation energies of GEM (*anti-anti* and *syn-anti* conformers) and PARA compared to experimental values obtained from the gas-phase absorption spectra. Values are given in [eV].

	GEM		PARA		
	calcd <i>anti-anti</i>	calcd <i>syn-anti</i>	exptl	calcd <i>anti-anti</i>	exptl
$S_1 (\pi \rightarrow \pi^*)$	4.17	4.17	4.0	4.15	4.0
$S_2 (\pi \rightarrow \pi^*)$	4.38	4.38	4.3	4.40	4.3
$S_3 (\pi \rightarrow \pi^*)$	4.59	4.59	4.98	4.64	4.98

experimental values obtained from the maxima in the absorption spectrum. The reader is referred to Heilbronner and Yang<sup>[39]</sup> for a thorough description of the electronic structure of paracyclophanes. The orbitals involved in the most important configurations in the excited states of the *anti-anti* conformer are shown in Figure 4. The orbitals for the *syn-anti* conformer are very similar. From the perspective of the individual halves of the molecule, calculations predict the  $S_1$  state to be quite similar to the  $S_1$  state of styrene, with HOMO–1  $\rightarrow$  LUMO and HOMO  $\rightarrow$  LUMO+1 being the most important configurations.<sup>[40]</sup> The  $S_2$  state is described by numerous configurations and no simple characterization can be made. The  $S_3$  state is mainly a HOMO  $\rightarrow$  LUMO excitation. Note that in the HOMO there is a nodal plane between the styrene units, whereas in the LUMO there is not. Furthermore, as can be seen from the perspective of the ethylene groups, the HOMO  $\rightarrow$  LUMO excitation is analogous to the  $\pi \rightarrow \pi^*$  excitation that leads to the ethylene dimerization. Thus, we expect the HOMO  $\rightarrow$  LUMO excitation to describe the diabatic state that is reactive in the [2+2] cycloaddition.

According to the Woodward–Hoffmann rules pericyclic reactions that are forbidden in the ground state are allowed

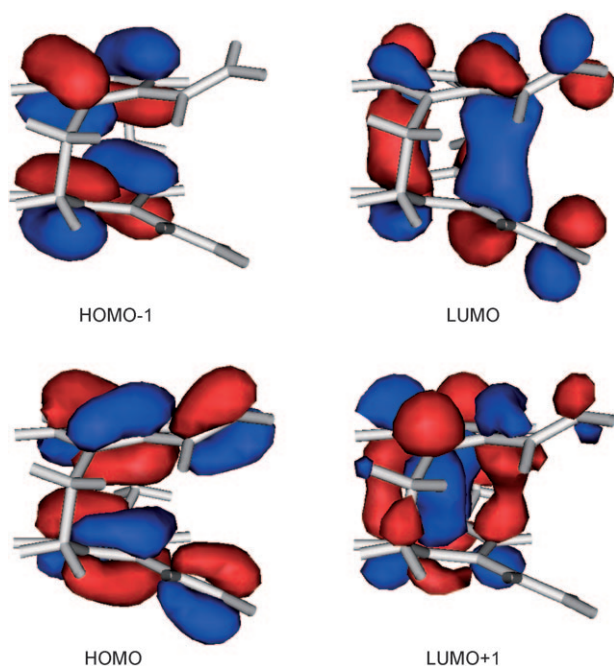


Figure 4. RI-CC2/cc-pVDZ orbitals calculated at the FC geometry in the *anti-anti* conformer of GEM.

in the excited state (e.g., Ref. [41], and references cited therein). In the case of ethylene dimerization, computations do indeed predict the pericyclic reaction to occur through a conical intersection between  $S_1$  and  $S_0$ .<sup>[41,42]</sup> Therefore, a search for a conical intersection (CI) between  $S_1$  and  $S_0$  leading to [2+2] cycloaddition was conducted. The resulting geometry and branching space vectors are shown in Figure 5. The geometry is quite similar to the corresponding CI geometry calculated for the ethylene dimerization.<sup>[41,42]</sup> The major difference is the asymmetry present in the carbon–carbon distances of the forming single bonds (1.98 and 2.55 Å), compared to the value of 2.19 Å computed for the ethylene dimerization.<sup>[42]</sup> Considering a more dynamical

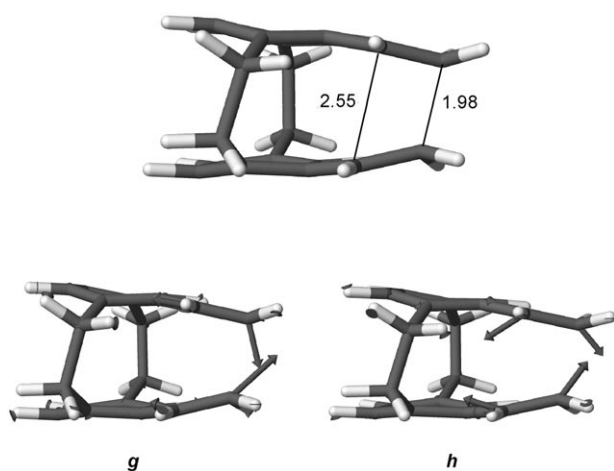


Figure 5. The geometry, gradient difference ( $g$ ) and derivative coupling ( $h$ ) vectors at the  $S_1/S_0$  CI in GEM. Distances are measured in [Å].

aspect of the [2+2] cycloaddition in GEM, following the gradient difference and derivative coupling vectors towards the CI primarily leads to an approach of the outer carbon–carbon pair in the forming cyclobutane ring, which further emphasizes the asymmetry of the reaction. The asymmetry is most likely due to the presence of the rigid paracyclophane scaffold that makes it unfavorable to obtain a geometry with symmetrical C–C bond lengths. This implies that the bond formation in the [2+2] reaction in GEM is asymmetrical, which in the most extreme case would mean that the reaction is not concerted, but stepwise with a biradical intermediate in the ground state. It was not possible to locate such an intermediate, though, as CAS (4,4) geometry optimization started close to the CI clearly converged towards the cyclobutane product.

The quasi-diabatic potential energy curves along the linearly interpolated [2+2] cycloaddition reaction path in the *anti-anti* conformer of GEM are shown in Figure 6. It is ap-

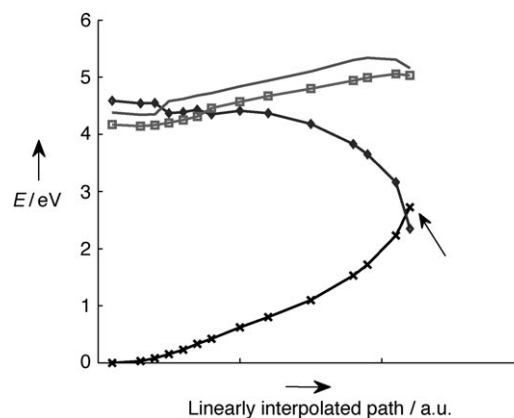


Figure 6. RI-CC2/cc-pVDZ potential energy curves along the linearly interpolated reaction path from the FC to the CI geometry in the *anti-anti* conformer of GEM. The excited-state curves are constructed so as to represent approximately diabatic states  $S_a$  ( $\blacklozenge$ ),  $S_b$  ( $\blacksquare$ ), and  $S_c$  ( $\square$ ) ( $S_0 = \times$ ). The  $S_1/S_0$  CI is marked by the arrow.

parent that the reactive diabatic state is  $S_a$  (the  $S_3$  adiabatic state in the FC region), agreeing with our expectations based on the discussion above. The interpolated reaction path in the  $S_1$  adiabatic state involves a small barrier of  $\approx 0.2$  eV of electronic energy. One should keep in mind, though, that the minimum energy path could be different from the linearly interpolated one and, thus, not involve a barrier. Calculating a reliable minimum energy path using SA-CASSCF would be prohibitively computationally expensive, though, because a reasonable active space should include all the sixteen  $\pi$  electrons. Furthermore, when taking the momentum of the wave packet into account it is not necessarily so that the minimum energy path will be the one followed, because inertia also plays a role, as seen for example in the variation of  $S_1$  lifetimes in  $\alpha,\beta$ -enones.<sup>[43]</sup> Such dynamical effects can only be correctly addressed computationally by molecular dynamics simulations.

*Pseudo-para-divinyl[2.2]paracyclophane*: The calculated geometry of PARA (not shown) is very similar to the geometry of the corresponding crystal structure (see above). As opposed to the case of GEM there is a quite good agreement between the vinyl-group twist angle of the calculated and the crystal structure, the values being 24° and 29°, respectively. As discussed for GEM, we do not find that further detailed comparison of the calculated and crystal structures is justified. In contrast to GEM, PARA is symmetric and possesses  $C_i$  symmetry. A scan of the twist angle, while relaxing all other parameters, was performed. The scan revealed that the electronic energies of the  $C_i$  geometry and the  $C_1$  geometry, in which one vinyl group is twisted in the opposite direction, are identical (within 1 meV). Furthermore, there is virtually no barrier separating them. Thus, in the gas phase at elevated temperatures, conformers covering a broad range of twist angles are expected to be present, effectively reducing the symmetry of the molecule to  $C_1$ .

Excited states were calculated and the three lowest excitation energies are shown in Table 1. Their predicted electronic characters are very similar to the corresponding states in GEM, agreeing with the similarity of the absorption spectra of the compounds.

**Time-resolved photoelectron spectra:** Ionization occurs to the ionic ground state, for which the ionization potentials (IPs) were previously determined by He<sup>I</sup> photoelectron spectroscopy to 7.8 and 7.9 eV for GEM and PARA, respectively.<sup>[44]</sup> In the two experiments with pump wavelengths of  $\lambda_p = 249$  and 300 nm, and a probe wavelength of  $\lambda_e = 400$  nm, the total energies of one pump and two-probe-photons are 11.2 eV and 10.3 eV, respectively. Time constants and decay-associated photoelectron spectra were determined by fitting the TRPES data set  $S(\Delta t, E)$  to the following expression [Eq. (1)], by using a Levenberg–Marquart global fitting routine:

$$S(\Delta t, E) = \sum_i A_i(E) P_i(\Delta t) \otimes g(\Delta t) \quad (1)$$

where the decay-associated spectrum  $A_i(E)$  represents the fitted amplitudes across the kinetic energy spectrum of the time-dependent population  $P_i(\Delta t)$  of the  $i$ th channel, convolved with the experimentally determined Gaussian cross-correlation  $g(\Delta t)$ . For details see reference [45]. In the following, we define normalized decay-associated spectra as decay-associated spectra that have been normalized to have a maximum amplitude of 1.

*Pseudo-para-divinyl[2.2]paracyclophane*: For PARA, only data with  $\lambda_p = 249$  nm and  $\lambda_e = 400$  nm were recorded. The resulting time-resolved photoelectron (TRPE) spectrum is shown in Figure 7. From the IP and the total photon energy, the maximum kinetic energy of the photoelectrons in the one-pump-plus-two-probe-photon ([1,2']) ionization scheme is 3.3 eV. The region of the spectrum corresponding to [1,1'] ionization, below 0.2 eV, is not considered. The data analysis

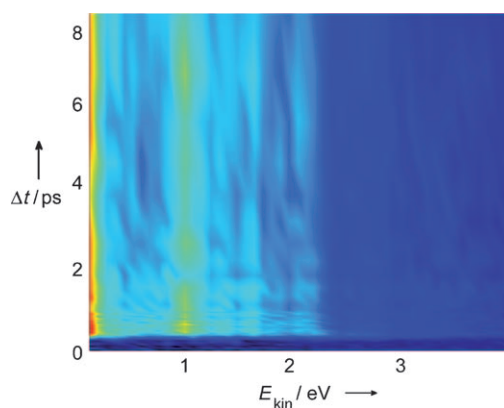


Figure 7. TRPE spectrum of PARA excited at  $\lambda_p = 249$  nm and probed at  $\lambda_e = 400$  nm.

focuses on the region between 0.5–3.3 eV. The PE spectrum is broad and has no obvious structure. This is in agreement with the computational finding that a broad range of vinyl-group twist angles gives rise to an extended range of conformations, leading to an inhomogeneous broadening of the PE spectrum.

The low-kinetic-energy region, below 2 eV, is delayed as compared to the high-energy region above 2 eV (not visible in Figure 7 due to the time scaling). This is the signature of a lower lying state being populated by internal conversion from the initial state excited at the FC geometry. The internal conversion converts electronic to vibrational energy, thereby shifting the signal to lower kinetic energies. Fitting the TRPE spectrum as described above, gave three time constants of  $(50 \pm 30)$  fs,  $(0.6 \pm 0.3)$  ps, and  $> 500$  ps, and the decay-associated spectra of these three channels are shown in Figure 8. The third time constant was too long to be reasonably estimated from the fit, but a lower bound of 500 ps can be stated. As can be seen, the rise time of the delayed part of the spectrum—corresponding to the region of the

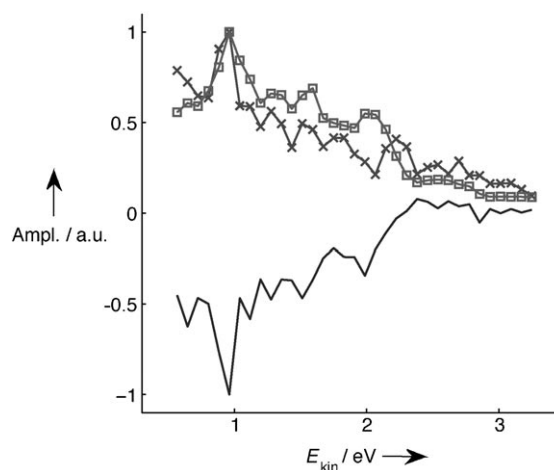


Figure 8. Normalized decay-associated spectra obtained from the global fit of the TRPE spectrum of PARA excited at  $\lambda_p = 249$  nm and probed at  $\lambda_e = 400$  nm (— = 50 fs, × = 0.6 ps, and ■ = > 500 ps).

decay-associated spectrum that has a negative amplitude—is 50 fs. The intermediate state in the scheme has a lifetime of 0.6 ps, decaying to a much longer lived species with a lifetime of more than 500 ps.

*Pseudo-gem-divinyl[2.2]paracyclophane*: From the IP and the total photon energies, the maximum kinetic energy of photoelectrons from GEM is 3.4 and 2.5 eV for the  $\lambda_p=249$  and 300 nm experiment, respectively. Thus, these are the cutoffs below which the temporal evolution of the TRPE spectra in Figure 9 has been analyzed. As can be seen, the spectra are very similar to the ones of PARA.

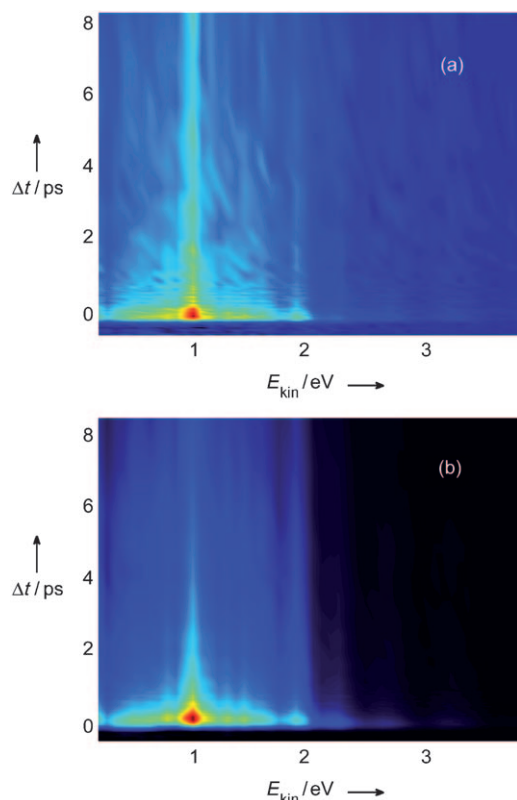


Figure 9. TRPE spectra of GEM excited at a)  $\lambda_p=300$  and b) 249 nm, both probed at  $\lambda_e=400$  nm.

As was the case for PARA in the  $\lambda_p=249$  nm experiment, electrons can also be generated from a  $[1,1']$  ionization 0.3 eV above the IP. Thus, the data analysis has been focused on the region between 0.3–3.4 eV, which corresponds to a  $[1,2']$  ionization. As found for PARA, the low-energy region of the spectrum is delayed in time as compared to the high-energy region, indicating a sequential process. Time constants and decay-associated spectra were determined by fitting the TRPE spectrum in the same way as for PARA. The resulting three time constants are  $(120 \pm 30)$  fs,  $(330 \pm 50)$  fs, and  $(8.2 \pm 0.9)$  ps, and the decay-associated spectra for these three channels are shown in Figure 10. As can be seen, the rise time of the delayed part of the spectrum is 120 fs. Im-

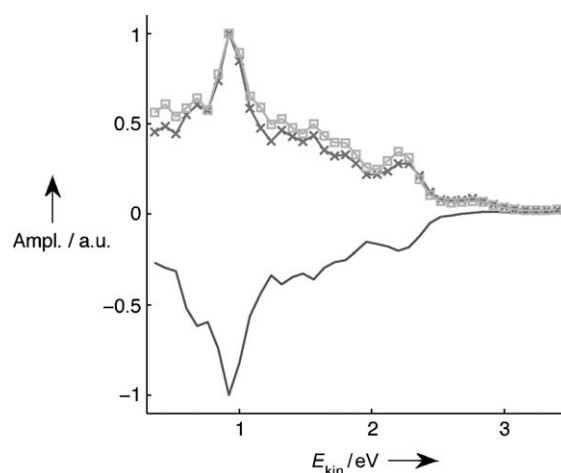


Figure 10. Normalized decay-associated spectra obtained from the global fit of the TRPE spectrum of GEM excited at  $\lambda_p=249$  nm and probed at  $\lambda_e=400$  nm (— = 120 fs,  $\times$  = 330 fs, and  $\blacksquare$  = 8.2 ps).

portantly, the time constant of the last step is 8.2 ps, much shorter than the  $>500$  ps for the same step in PARA.

For the  $\lambda_p=300$  nm data (see Figure 9a) there are no time-delayed features in the TRPE spectrum. Time constants and decay-associated spectra were determined by fitting the region of the TRPE spectrum below 2.5 eV in the same manner as it was done for the  $\lambda_p=249$  nm data described above. The resulting three time constants are  $(340 \pm 50)$  fs,  $(13.5 \pm 1.0)$  ps, and  $(400 \pm 50)$  ps, and the decay-associated spectra for these three channels are shown in Figure 11.

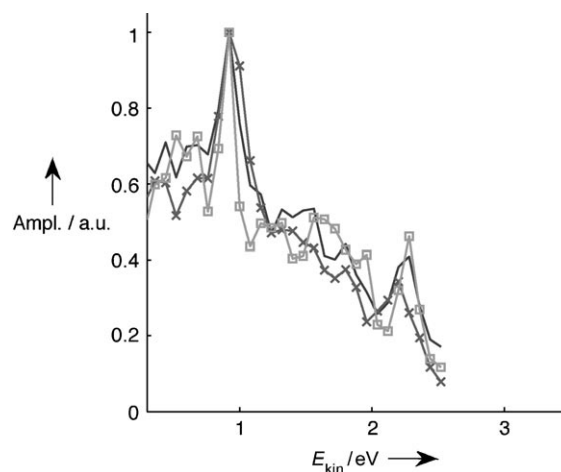
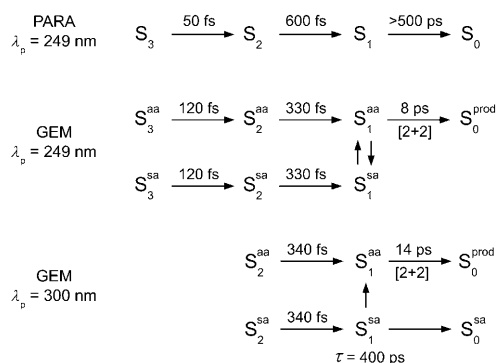


Figure 11. Normalized decay-associated spectra obtained from the global fit of the TRPE spectrum of GEM excited at  $\lambda_p=300$  nm and probed at  $\lambda_e=400$  nm (— = 340 fs,  $\times$  = 13 ps, and  $\blacksquare$  = 400 ps).

## Discussion

*Pseudo-para-divinyl[2.2]paracyclophane*: The rise time, 50 fs, obtained from the fit of the TRPE spectrum, is assigned to population of the  $S_2$  and the  $S_1$  state from the ini-

tially excited  $S_3$  state. Because these states have overlapping PE spectra, it is not possible to assign whether the dynamics are sequential—population of  $S_2$  followed by a decay to  $S_1$ —or parallel—population of both  $S_2$  and  $S_1$  from  $S_3$ . We assign the 0.6 ps decay to the lifetime of the  $S_2$  state, whereas the subsequent long-lived decay,  $> 500$  ps, is attributed to the lifetime of the  $S_1$  state. This interpretation of the decay dynamics is shown schematically in Scheme 3, assuming se-



Scheme 3. The reaction dynamics in PARA and GEM as interpreted from the TRPE data. The symbols  $S_x^{aa}$  and  $S_x^{sa}$  represent state  $x$  in the *anti-anti* and *syn-anti* conformer, respectively.  $S_0^{prod}$  refers to the ground-state product of the [2+2] cycloaddition. The lifetime of the  $S_1^{sa}$  state, which decays by two different pathways, is indicated by  $\tau$ .

quential population of the  $S_2$  and the  $S_1$  state. The  $S_1$  lifetime in PARA is significantly longer than the styrene  $S_1$  state lifetime of 88 ps,<sup>[46]</sup> but similar to the 100–300 ps lifetime of the  $S_1$  state in the benzene dimer.<sup>[47]</sup> Assuming that the  $S_1 \rightarrow S_0$  population decay pathway of PARA is similar to the one of styrene and other substituted benzenes, the reason for the long  $S_1$  lifetime could be the rigidity of the paracyclophane cage structure, which restricts the out of plane motions of the benzene ring that lead to the  $S_1/S_0$  CI.<sup>[46–48]</sup>

### Pseudo-gem-divinyl[2.2]paracyclophane

*Exciting the  $S_1$  and  $S_2$  state directly:* In the  $\lambda_p = 300$  nm experiment both the  $S_1$  and the  $S_2$  state can be excited by the pump pulse. Thus, the TRPE spectrum is expected to reflect dynamics evolving in both states in parallel. From a kinetics perspective, this would give rise to a bi-exponential decay. This is indeed observed. The fact that the decay-associated spectra are identical can be explained by ionization through an intermediate state, that is, the absorption of the first of the two probe-photons is resonant. Thus, the decay-associated spectra are identical because they represent the PE spectrum of the intermediate highly excited state. We assign the 340 fs to the lifetime of the  $S_2$  state. The two long time constants, 13.5 and 400 ps, are assigned to the lifetime of the  $S_1$  state in the *anti-anti* and *syn-anti* conformer, respectively. This assignment is depicted schematically in Scheme 3, where, for simplicity, only sequential population of  $S_1$  is

shown. The interpretation is supported by the fact that the mean value of the ratios of the 13.5 and 400 ps decay amplitudes is 3.4, fairly close to the 3:1 *anti-anti/syn-anti* conformer ratio measured in the crystal structure (see above). One possible explanation for the relatively long lifetime of the  $S_1$  state in the reactive *anti-anti* conformer is the presence of a barrier along the [2+2] reaction coordinate, as predicted by the calculations. The 400 ps lifetime of the *syn-anti* conformer agrees well with the  $> 500$  ps lifetime of the  $S_1$  state in PARA. However, the fact that the  $S_1$  lifetime is shorter in the *syn-anti* conformer of GEM excited at 300 nm as compared to PARA excited at 249 nm, gives some evidence that the ethylene group might cross the rotational barrier to form the *anti-anti* conformer, thus providing an additional decay channel that is not present in PARA.

*Exciting the  $S_3$  state:* The 120 fs rise time obtained from the fit of the TRPE spectrum measured when using  $\lambda_p = 249$  nm is assigned to population of the  $S_2$  and the  $S_1$  state from the initially excited  $S_3$  state. As was the case for PARA, these states have overlapping PE spectra, so it is not possible to decide whether the dynamics are sequential or parallel. The decays are interpreted as described in the previous section; the short time constant is the lifetime of the  $S_2$  state, whereas the longer one is that of the  $S_1$  state (see Scheme 3). Note that the  $S_2$  lifetime, 330 fs, is almost identical to that observed when exciting the  $S_2$  state directly, despite the fact that the vibrational energy content is approximately 0.7 eV higher in the former experiment. We assigned this to be a signature of nonadiabatic ultrafast dynamics, where population transfer is poorly described by density-of-states-based models, such as the Fermi Golden rule, because it is determined by the momentum in a small subset of the vibrational coordinates.<sup>[43,45,49,50]</sup>

In this experiment we do not observe a bi-exponential decay of  $S_1$ . We believe that this is because both conformers exhibit an  $S_1$  lifetime of very similar magnitude. Considering that the vibrational excess energy in the  $S_1$  state when populated from the  $S_3$  state is approximately 1 eV, we find it likely that the rotational barrier of the vinyl group can now be crossed on a shorter timescale, bringing the molecule into the reactive *anti-anti* conformation in which [2+2] cycloaddition commences through the  $S_1/S_0$  CI. In the framework of intramolecular vibrational-energy redistribution (IVR) this is indeed plausible. Thus, the vinyl-group rotation is a low-frequency mode that, because of a high density of states, is favored when IVR commences in the  $S_1$  state of the *syn-anti* conformer. Assuming that the  $S_1$  lifetime of both conformers is similar, it means that the rate of conversion of the *syn-anti* to the *anti-anti* conformer is faster than the rate of the [2+2] cycloaddition. The lifetime, 8.2 ps, is shorter than that observed for direct excitation of  $S_1$  in the  $\lambda_p = 300$  nm experiment, 13.5 ps. This shortening of the lifetime can be explained by the higher vibrational energy content when  $S_1$  is populated from the higher-lying electronic state. The higher vibrational energy content might mean that the barrier towards the  $S_1/S_0$  CI (in the present case

leading to a [2+2] cycloaddition) is crossed faster, as was previously observed for substituted benzenes.<sup>[46]</sup>

## Conclusion

The first study of a pseudo-bimolecular [2+2] cycloaddition in the gas phase was performed by using time-resolved photoelectron spectroscopy. Use of the [2.2]paracyclophane scaffold made it possible to place two ethylene units at a distance from which the pseudo-bimolecular reaction can take place. Thus, pseudo-*gem*-divinyl[2.2]paracyclophane was chosen as a model system. Two conformers of the molecule, the *anti-anti* conformer, which is reactive in [2+2] cycloaddition, and the *syn-anti* conformer, which is not, were identified with X-ray diffraction measurements of the solid sample. The presence of these two types of conformers makes the molecule an ideal system for an investigation of the relation between ground-state conformation (determining the Franck–Condon geometry) and excited-state reactivity in a [2+2] photocycloaddition. Experiments were also performed on the reference compound pseudo-*para*-divinyl[2.2]paracyclophane, in which the ethylene units cannot react through [2+2] cycloaddition. The S<sub>1</sub> state in PARA has a lifetime of more than 500 ps. When exciting the S<sub>1</sub> state in GEM directly, the two conformers seem to exhibit quite different lifetimes; 13.5 ps in the *anti-anti* and 400 ps in the *syn-anti* conformer. This result shows the importance of the molecular conformation prior to light absorption in inducing a [2+2] cycloaddition: the S<sub>1</sub> lifetime in the non-reactive *syn-anti* conformation is significantly longer than in the reactive *anti-anti* conformation. Furthermore, the experiments show that it is only the lifetime of the S<sub>1</sub> state, in which the calculations predict the [2+2] cycloaddition to occur through a S<sub>1</sub>/S<sub>0</sub> conical intersection, which is significantly affected by the vicinity of the ethylene units. Accordingly, the observed S<sub>3</sub> and S<sub>2</sub> state lifetimes of GEM and PARA do not differ much.

With respect to the [2+2] cycloaddition leading to thymine dimerization in DNA, a conformation which is non-reactive in [2+2] cycloaddition will be crucial because it allows for electronic relaxation mechanisms to efficiently compete with the harmful thymine dimerization channel. Thus, extrapolating from the findings of this work, it would seem that the ground-state conformation before light absorption is just as important as the relaxation mechanisms in protecting DNA from photodamage, consistent with the suggestions of Schreier et al.<sup>[15]</sup>

## Experimental Section

The pseudo-*gem* and pseudo-*para* isomers of divinyl[2.2]paracyclophane were synthesized as described by Hopf and coworkers.<sup>[22,51]</sup>

**Experimental setup:** The UV/Vis gas-phase absorption spectra were recorded with a Varian 5e spectrophotometer by subliming the solid at 140–150 °C into a homemade evacuated quartz cell with a light path length of 10 cm.

TRPES experiments were performed by combining a femtosecond laser system with a supersonic molecular beam magnetic bottle time-of-flight photoelectron spectrometer. The molecular beam magnetic bottle apparatus has been described in detail elsewhere.<sup>[52]</sup>

The femtosecond laser system consisted of a Ti:sapphire oscillator (Spectra Physics, Tsunami, 80 MHz, 800 nm, 80 fs) pumped by a Nd:YLF diode laser (Spectra Physics, Millennia). The output of the oscillator was amplified by a Ti:sapphire regenerative amplifier (Coherent, Legend, 1 kHz, 130 fs) pumped by two Nd:YLF lasers (Positive Light, Evolution). Femtosecond laser pulses of wavelengths  $\lambda_p=249$  or 300 nm were used in the pump step of the experiment. Pulses of  $\lambda_p=249$  nm were generated by noncollinear sum frequency mixing of the fundamental with the output of an optical parametric amplifier (TOPAS, Light Conversion), followed by frequency doubling. Pulses of  $\lambda_p=300$  nm were generated by the fourth harmonic of the output of a second TOPAS. For the probe step the second harmonic ( $\lambda_c=400$  nm) of the fundamental was used. Pulse energies for  $\lambda_p=249$  and 300 nm, and  $\lambda_c=400$  nm were 1.5, 1.7, and 15–25  $\mu\text{J}$ , respectively. The pulses were focused mildly into the interaction region by an  $f/100$  concave Al mirror. Estimated pulse intensities were  $1 \times 10^{12}$   $\text{W cm}^{-2}$  for the pump pulses and  $5\text{--}9 \times 10^{12}$   $\text{W cm}^{-2}$  for the probe pulses.

The temporal cross correlation between the pump and probe pulse in the  $\lambda_p=249$  nm,  $\lambda_c=400$  nm experiment was measured by the rise time of diazabicyclo[2.2.2]octane ionized by one-pump-plus-one-probe-photon ([1,1']) and was determined to be  $(130 \pm 10)$  fs. Because the cycloaddition experiments were performed by using [1,2'] ionization, this value was reduced by a factor of  $\sqrt{3/2}$  to  $(115 \pm 10)$  fs assuming Gaussian pulses of identical length. The temporal cross correlation in the  $\lambda_p=300$  nm,  $\lambda_c=400$  nm experiment was measured by using [1,2'] ionization of *trans*-1,3-butadiene and was determined to be  $(130 \pm 10)$  fs. The time delay between the pump and the probe pulse was computer controlled by a motorized linear translation stage. At each time delay, the pump–probe signal was determined from the total signal by subtracting the background signal due to electrons generated by the pump and probe pulses alone.

In the interaction region, a high-intensity, supersonic molecular beam propagated perpendicular to the incoming laser pulses. The beam was generated by a 1 kHz Even–Lavie valve with a 250  $\mu\text{m}$  diameter conical nozzle. Helium was used as carrier gas with a backing pressure of 3 kTorr. The solid sample was introduced into the body of the valve and sublimed by heating the valve to 110–120 °C. To prevent condensation of solid sample in the valve opening, the nozzle was heated by a separate heater to keep its temperature approximately 20 °C higher than the temperature of the body, but still below the decomposition temperature of the compounds. The photoelectron kinetic energies were calibrated by using the known photoelectron spectrum of NO.<sup>[53]</sup>

**Computational details:** Ground-state-optimized geometries and frequencies were determined at the B3LYP/6-31G(d) level of theory by using Gaussian 03.<sup>[54]</sup> TURBOMOLE V5.8 was used to calculate RI-CC2/cc-pVDZ vertical excitation energies<sup>[55,56]</sup> at these geometries. State-averaged complete active space self-consistent field (SA-CASSCF) calculations have been performed by using MOLPRO 2008.1.<sup>[57]</sup> A search for a CI between S<sub>1</sub> and S<sub>0</sub> in the *anti-anti* conformer of GEM was performed by using SA-CASSCF(4,4)/6-31G(d). A transition state for the [2+2] cycloaddition in the ground state was located by using HF/6-31G(d) and was used as a starting point in the search for the CI. The active space in the CAS calculation consisted of four electrons distributed among the two highest occupied  $\pi$  orbitals and the two lowest unoccupied  $\pi^*$  orbitals. An excited-state [2+2] cycloaddition reaction path was approximated by a linear interpolation in internal coordinates between the ground-state geometry and the geometry at the CI. Single-point excitation energies were calculated along the path by using RI-CC2/cc-pVDZ.

### X-ray single-crystal diffraction

#### GEM

*Crystal data:* C<sub>20</sub>H<sub>20</sub>, M<sub>r</sub>=260.36, monoclinic, P2<sub>1</sub>/c, a=7.5693(3), b=11.1089(4), c=16.8257(6) Å,  $\beta=100.518(2)^\circ$ , V=1391.04 Å<sup>3</sup>, Z=4,  $\lambda(\text{MoK}\alpha)=0.71073$  Å.

**Data collection:** A colorless plate (ca.  $0.45 \times 0.35 \times 0.20$  mm) was mounted on a Bruker Kappa APEXII diffractometer. A total of 28853 data were recorded to  $2\theta$   $66^\circ$ , of which 5244 were independent ( $R_{\text{int}} = 0.023$ ).

**Structure refinement:** The structure was refined by using SHELXL-97.<sup>[58]</sup> For the disordered carbon atoms the bond distances, bond angles, and thermal parameters were restrained to expected values. The hydrogen atoms that were attached to fully occupied carbon atoms were located on difference maps and refined isotropically. The remaining hydrogen atoms were placed in calculated positions and refined by using a riding model. The final  $R2$  (all reflections) was 0.126 for all intensities and 311 parameters (160 restraints) with  $R1$  ( $I > 2\sigma(I)$ ) 0.042;  $S$  1.05.

#### PARA

**Crystal data:**  $C_{20}H_{20}$ ,  $M_r = 260.36$ , triclinic,  $P\bar{1}$ ,  $T = -173^\circ\text{C}$ ,  $a = 8.1557(4)$ ,  $b = 8.9210(4)$ ,  $c = 10.7187(5)$  Å,  $\alpha = 69.715(5)$ ,  $\beta = 77.906(5)$ ,  $\gamma = 74.628(5)^\circ$ ,  $V = 699.27$  Å<sup>3</sup>,  $Z = 2$  (two independent molecules, each with inversion symmetry),  $\lambda(\text{MoK}\alpha) = 0.71073$  Å.

**Data collection:** A colorless block (ca.  $0.4 \times 0.35 \times 0.35$  mm) was mounted on an Oxford Diffraction Xcalibur E diffractometer. A total of 58433 data were recorded to  $2\theta$   $60^\circ$ , of which 4036 were independent ( $R_{\text{int}} = 0.030$ ).

**Structure refinement:** The structure was refined by using SHELXL-97.<sup>[58]</sup> Hydrogen atoms were included by using a riding model. The final  $R2$  (all reflections) was 0.122 for all intensities and 181 parameters, with  $R1$  ( $I > 2\sigma(I)$ ) 0.041;  $S$  0.94.

CCDC-788032 (GEM) and 788033 (PARA) contain the supplementary crystallographic data for this paper. These data can be obtained free of charge from The Cambridge Crystallographic Data Centre via [www.ccdc.cam.ac.uk/data\\_request/cif](http://www.ccdc.cam.ac.uk/data_request/cif).

## Acknowledgements

R.Y.B. acknowledges financial support from the Niels Bohr Foundation, the Royal Danish Academy of Science and Letters. O.S. thanks the Humboldt Foundation for financial support. Dr. Michael Schuurman and Dr. Serguei Patchkovskii are thanked for helpful discussions regarding the ab initio calculations.

- [1] C. E. Crespo-Hernández, B. Cohen, P. M. Hare, B. Kohler, *Chem. Rev.* **2004**, *104*, 1977–2020.
- [2] C. T. Middleton, K. de La Harpe, C. Su, Y. K. Law, C. E. Crespo-Hernández, B. Kohler, *Annu. Rev. Phys. Chem.* **2009**, *60*, 217–239.
- [3] S. Perun, A. L. Sobolewski, W. Domcke, *J. Phys. Chem. A* **2006**, *110*, 9031–9038.
- [4] H. Satzger, D. Townsend, M. Zgierski, S. Patchkovskii, S. Ullrich, A. Stolow, *Proc. Natl. Acad. Sci. USA* **2006**, *103*, 10196–10201.
- [5] L. Serrano-Andrés, M. Merchán, *J. Photochem. Photobiol. C* **2009**, *10*, 21–32.
- [6] C. Z. Bisgaard, H. Satzger, S. Ullrich, A. Stolow, *ChemPhysChem* **2009**, *10*, 101–110.
- [7] S. Ullrich, T. Schultz, M. Z. Zgierski, A. Stolow, *Phys. Chem. Chem. Phys.* **2004**, *6*, 2796–2801.
- [8] S. Ullrich, T. Schultz, M. Z. Zgierski, A. Stolow, *J. Am. Chem. Soc.* **2004**, *126*, 2262–2263.
- [9] S. Brondsted Nielsen, T. I. Sølling, *ChemPhysChem* **2005**, *6*, 1276–1281.
- [10] H. R. Hudock, B. G. Levine, A. L. Thompson, H. Satzger, D. Townsend, N. Gador, S. Ullrich, A. Stolow, T. J. Martínez, *J. Phys. Chem. A* **2007**, *111*, 8500–8508.
- [11] J. Cadet, P. Vigny, *Bioorganic Photochemistry, Vol. 1* (Ed.: H. Morrison), **1990**, pp. 1–272.
- [12] T. Douki, A. Reynaud-Angelin, J. Cadet, E. Sage, *Biochemistry* **2003**, *42*, 9221–9226.
- [13] J. S. Taylor, *Acc. Chem. Res.* **1994**, *27*, 76–82.
- [14] A. A. Vink, L. Roza, *J. Photochem. Photobiol. B* **2001**, *65*, 101–104.
- [15] W. J. Schreier, T. E. Schrader, F. O. Koller, P. Gilch, C. E. Crespo-Hernández, V. N. Swaminathan, T. Carell, W. Zinth, B. Kohler, *Science* **2007**, *315*, 625–629.
- [16] P. J. Wagner, *Acc. Chem. Res.* **1983**, *16*, 461–467.
- [17] C. Kötting, E. W. Diau, T. I. Sølling, A. H. Zewail, *J. Phys. Chem. A* **2002**, *106*, 7530–7546.
- [18] R. Y. Brogaard, K. B. Møller, T. I. Sølling, *J. Phys. Chem. A* **2008**, *112*, 10481–10486.
- [19] R. Y. Brogaard, T. I. Sølling, *J. Mol. Struct.: THEOCHEM* **2007**, *811*, 117–124.
- [20] N. Rusteika, R. Y. Brogaard, T. I. Sølling, F. M. Rudakov, P. M. Weber, *J. Phys. Chem. A* **2009**, *113*, 40–43.
- [21] M. Rosenberg, T. I. Sølling, *Chem. Phys. Lett.* **2010**, *484*, 113–118.
- [22] L. Bondarenko, S. Hentschel, H. Greiving, J. Grunenberg, H. Hopf, I. Dix, P. G. Jones, L. Ernst, *Chem. Eur. J.* **2007**, *13*, 3950–3963.
- [23] M. Seel, W. Domcke, *J. Chem. Phys.* **1991**, *95*, 7806–7822.
- [24] B. Kim, C. P. Schick, P. M. Weber, *J. Chem. Phys.* **1995**, *103*, 6903–6913.
- [25] T. Seideman, *Annu. Rev. Phys. Chem.* **2002**, *53*, 41–65.
- [26] D. M. Neumark, *Annu. Rev. Phys. Chem.* **2001**, *52*, 255–277.
- [27] K. L. Reid, *Annu. Rev. Phys. Chem.* **2003**, *54*, 397–424.
- [28] A. Stolow, *Annu. Rev. Phys. Chem.* **2003**, *54*, 89–119.
- [29] A. Stolow, A. E. Bragg, D. M. Neumark, *Chem. Rev.* **2004**, *104*, 1719–1758.
- [30] M. Wollenhaupt, V. Engel, T. Baumert, *Annu. Rev. Phys. Chem.* **2005**, *56*, 25–56.
- [31] I. V. Hertel, W. Radloff, *Rep. Prog. Phys.* **2006**, *69*, 1897–2003.
- [32] T. Suzuki, *Annu. Rev. Phys. Chem.* **2006**, *57*, 555–592.
- [33] K. L. Reid, *Int. Rev. Phys. Chem.* **2008**, *27*, 607–628.
- [34] A. Stolow, J. G. Underwood, *Adv. Chem. Phys.* **2008**, *139*, 497–584.
- [35] G. F. Caramori, S. E. Galembeck, K. K. Laali, *J. Org. Chem.* **2005**, *70*, 3242–3250.
- [36] D. Henseler, G. Hohlneicher, *J. Phys. Chem. A* **1998**, *102*, 10828–10833.
- [37] H. Hope, J. Bernstein, K. N. Trueblood, *Acta Crystallogr. Sect. B* **1972**, *28*, 1733–1743.
- [38] T. Kobayashi, K. Yokota, S. Nagakura, *J. Electron Spectrosc. Relat. Phenom.* **1973**, *2*, 449–454.
- [39] E. Heilbronner, Z. Yang, *Top. Curr. Chem.* **1983**, *115*, 1–55.
- [40] J. W. Ribblett, D. R. Borst, D. W. Pratt, *J. Chem. Phys.* **1999**, *111*, 8454–8461.
- [41] F. Bernardi, S. De, M. Olivucci, M. A. Robb, *J. Am. Chem. Soc.* **1990**, *112*, 1737–1744.
- [42] M. Dallos, H. Lischka, R. Shepard, D. R. Yarkony, P. G. Szalay, *J. Chem. Phys.* **2004**, *120*, 7330–7339.
- [43] A. M. D. Lee, J. D. Coe, S. Ullrich, M. Ho, S. Lee, B. Cheng, M. Z. Zgierski, I. Chen, T. J. Martinez, A. Stolow, *J. Phys. Chem. A* **2007**, *111*, 11948–11960.
- [44] Z. Yang, E. Heilbronner, H. Hopf, S. Ehrhardt, S. Hentschel, *J. Phys. Chem.* **1988**, *92*, 914–917.
- [45] O. Schalk, A. E. Boguslavskiy, A. Stolow, *J. Phys. Chem. A* **2010**, *114*, 4058–4064.
- [46] S. Lee, K. Tang, I. Chen, M. Schmitt, J. P. Shaffer, T. Schultz, J. G. Underwood, M. Z. Zgierski, A. Stolow, *J. Phys. Chem. A* **2002**, *106*, 8979–8991.
- [47] W. Radloff, T. Freudenberger, H. H. Ritze, V. Stert, F. Noack, I. V. Hertel, *Chem. Phys. Lett.* **1996**, *261*, 301–306.
- [48] B. Lasorne, F. Sicilia, M. J. Bearpark, M. A. Robb, G. A. Worth, L. Blancafort, *J. Chem. Phys.* **2008**, *128*, 124307.
- [49] E. W. Diau, C. Kötting, T. I. Sølling, A. H. Zewail, *ChemPhysChem* **2002**, *3*, 57–78.
- [50] T. I. Sølling, E. W. Diau, C. Kötting, S. D. Feyter, A. H. Zewail, *ChemPhysChem* **2002**, *3*, 79–97.
- [51] H. Hopf, E. Herrmann, V. Raev, S. Ehrhardt, unpublished results.
- [52] S. Lochbrunner, J. J. Larsen, J. P. Shaffer, M. Schmitt, T. Schulz, J. G. Underwood, A. Stolow, *J. Electron Spectrosc. Relat. Phenom.* **2000**, *112*, 183–198.
- [53] G. K. Jarvis, M. Evans, C. Y. Ng, K. Mitsuke, *J. Chem. Phys.* **1999**, *111*, 3058–3069.

- [54] Gaussian 03, Revision C.02, M. J. Frisch, G. W. Trucks, H. B. Schlegel, G. E. Scuseria, M. A. Robb, J. R. Cheeseman, V. G. Zakrzewski, J. A. Montgomery, Jr., R. E. Stratmann, J. C. Burant, S. Dapprich, J. M. Millam, A. D. Daniels, K. N. Kudin, M. C. Strain, O. Farkas, J. Tomasi, V. Barone, M. Cossi, R. Cammi, B. Mennucci, C. Pomelli, C. Adamo, S. Clifford, J. Ochterski, G. A. Petersson, P. Y. Ayala, Q. Cui, K. Morokuma, D. K. Malick, A. D. Rabuck, K. Raghavachari, J. B. Foresman, J. Cioslowski, J. V. Ortiz, A. G. Baboul, B. B. Stefanov, G. Liu, A. Liashenko, P. Piskorz, I. Komaromi, R. Gomperts, R. L. Martin, D. J. Fox, T. Keith, C. Y. P. M. A. Al-Laham, A. Nanayakkara, C. Gonzalez, M. Challacombe, P. M. W. Gill, B. Johnson, W. Chen, M. W. Wong, J. L. Andres, C. Gonzalez, M. Head-Gordon, E. S. Replogle, J. A. Pople, Gaussian Inc., Wallingford, CT, **2004**.
- [55] C. Hättig, F. Weigend, *J. Chem. Phys.* **2000**, *113*, 5154–5161.
- [56] C. Hättig, A. Kohn, *J. Chem. Phys.* **2002**, *117*, 6939–6951.
- [57] MOLPRO, version 2008.1, a package of ab initio programs, H. Werner, P. J. Knowles, R. Lindh, F. R. Manby, M. Schütz, P. Celani, T. Korona, A. Mitrushenkov, G. Rauhut, T. B. Adler, R. D. Amos, A. Bernhardsson, A. Berning, D. L. Cooper, M. J. O. Deegan, A. J. Dobbyn, F. Eckert, E. Goll, C. Hampel, G. Hetzer, T. Hrenar, G. Knizia, C. Køppl, Y. Liu, A. W. Lloyd, R. A. Mata, A. J. May, S. J. McNicholas, W. Meyer, M. E. Mura, A. Nicklass, P. Palmieri, K. Pflüger, R. Pitzer, M. Reiher, U. Schumann, H. Stoll, A. J. Stone, R. Tarroni, T. Thorsteinsson, M. Wang, A. Wolf, **2008**, see: <http://www.molpro.net>.
- [58] G. Sheldrick, *Acta Crystallogr. Sect. A* **2008**, *64*, 112–122.

Received: October 11, 2010  
Published online: March 1, 2011